Do sun spots influence the onset of ENSO and PDO events in the Pacific Ocean?

Franklin Isaac Ormaza-González[1]*, and María Esther Espinoza-Celi*[1]

1) ESPOL Polytechnic University, Escuela Superior Politécnica del Litoral, ESPOL, (Facultad de Ingeniería Marítima, Ciencias Biológicas, Oceánicas y Recursos Naturales), Campus Gustavo Galindo Km. 30.5 Vía Perimetral, P.O. Box 09-01-5863, Guayaquil, Ecuador

Corresponding author: formaza@espol.edu.ec.

The sea surface temperature (SST), SST anomalies, ONI (Oceanographic El Niño Index) and MEI (Multivariate ENSO Index) in regions El Niño 1+2 (80°W-90°W, 0°-10°S) and 3.4 (5°N-5°S, 170°W-120°W) as well as the Pacific Decadal Oscillation (PDO) and Atlantic Multidecadal Oscillation (AMO) indexes, were correlated to sun spots number (SS) from cycles (SS#) 19 to 24 (1954-2017). Polynomial regression functions represented each of the six cycles with an average r^2>0.89 ($p<0.001$). Series of correlations between SS and chosen indices at different lag times (0, 6, 12, 24, 36 and 48 months) gave a response time of between 12 and 36 months. Over the entire 1954-2017 period, the SS cycles did not show a strong correlation with the variables or SST Anomaly in the El Niño areas 1+2 and 3.4. It seems that high and low SS balanced through the cycles. Improved correlations were found for the shorter period 1990-2016. The SST correlations against individual SS cycles in regions 3.4 and 1+2 were up to 0.219 (SS# 23) and <0.0675 (SS# 19) correspondingly. SST Anomaly, ONI and MEI correlated with r^2 of 0.250, 0.3943 and 0.2510, one-to-one; the lag time was 24-48 months and linear curves had positive slope. In general, more inconsistent and lower correlations were found in 1+2 than in 3.4. On longer time scale indexes, the PDO (as well as the AMO) seemed to respond in 36-48 months to SS cycles (r^2 of 0.625, SS# 19) and 0.766, SS# 24); whilst the AMO index gave a slightly lower correlation (0.490, SS# 20) with a similar lag time. Further analysis of SS numbers and the oceanic indices above during the ascending and descending phases of each cycle showed SST was best correlated with the ascending phase (up to r^2 of 0.870, with a lag time between SS cycle and index of about 36 months) and this trend also applied to the SST anomaly, although with slightly poorer correlations. The highest r^2 values coincided with strong ENSO events. The descending phase showed lower correlations between SS and ocean indices including MEI and ONI. The PDO was linearly correlated to SS (r^2 0.7677 to 0.2855 (12 to 24 months) as was the AMO (r^2 up to 0.700) whilst during descending phases correlations were poorer. The SS activity seemed to have a better correlation during the cold phase of PDO. These results show that warm events tend to occur in the ascending phase or at the top of the cycle, and have a delay time of around 36 months, whilst cold events are associated with descending phases but with a shorter lag time. The correlation analysis given here indicates sun spot activity should be considered as a factor that could condition and trigger low (PDO and AMO) and high (ONI-El Niño) frequency oceanographic events in the Pacific and Atlantic Oceans.

Key words: Sun spots cycles, SST, SSTA, ONI, MEI, PDO, AMO, El Niño, La Niña

Introduction.

Essentially, the only external source of energy to Earth is the sun, which constantly radiates a flux of energy to the upper atmosphere (the solar constant) of 1360 W m^{-2} or 1.36 kJ m^{-2} s^{-1} (Monteith, 1972) or 1.92 ly day^{-1} (Ormaza-González and Sanchez, 1983). Recently, Kopp and Lean (2011) have reported that the most accurate accepted solar constant value is 1360.8 ± 0.5 W m^{-2}. Of this flux of energy, 75-50 % reaches the Earth's surface (Ormaza-González and Sanchez, 1983; Lindsey, 2009) and the remainder is reflected and/or absorbed by clouds, particles, gases, etc. (Horning et al., 2003). About 90-93% of that energy reaching the surface is accumulated in the oceans (Trenberth et al., 2014; Clutz, 2017). The solar constant is affected by variations in sun spot (SS) number (Bhowmik and Nandy, 2018) and other solar activity parameters by around 0.1%, i.e. on the order of 1.361 W m^{-2}. The Hale cycle (around 11 years) is characterized by increasing and then decreasing SS numbers (Hathaway, 2015). Froelich (2013) suggested that the solar constant can vary by up to 4.0 W m^{-2} over two SS cycles, i.e. a 22-year cycle, and proposed a simple relationship between SS and the solar constant (SC), by assuming a direct relationship between the two

$SC = 1353.6 + 0.089\,(SS)$ (r^2 of 0.71, 95-99% confidence).

The surface-subsurface layers of the ocean that interact with the lower atmosphere alternately release and absorb heat energy. The work of Zhou and Tung (2010) reported the impact of the SC on global SST over 150 years, finding signals of cooling and warming SSTs at the valley and peak of the SS cycles. Schlesinger and Ramankutty (1994) reported a global cycle of 65-70 years that is possibly affected by greenhouse anthropogenic gases, sulphate aerosols and/or El Niño events, but they did not imply an external force such as the SS. There are well known oceanic events that are roughly periodic with low (25-30 years) or high (3-5 years) frequencies. These include the Pacific Decadal Oscillation (PDO, Mantua et al., 1997; Mantua and Hare, 2002; Zhang et al., 1997; Yim et al., 2013), Atlantic Multidecadal Oscillation (AMO, Enfield et al., 2001; Condron et al., 2005; Gray et al., 2010) and Interdecadal Pacific Oscillation (IPO, Henley et al., 2015), as well as El Niño (Busalacchi et al., 1983, see **COAPS Library's: http://www.coaps.fsu.edu/lib/biblio/coaps-a.html**) or La Niña (Yuan and Yan, 2012). During El Niño events, the surface and subsurface lose energy to the atmosphere and the opposite occurs during La Niña (Trenberth et al. 2014, Fasullo and Nerem, 2016); these events have a periodicity of 2-7 years while the decadal processes may take 25-30 years. The Interdecadal oscillations have a series of impacts; e.g., the PDO gives rise to teleconnections between the tropic and mid-latitudes (Yoon and Yeh, 2010), and the effects include: 1) the ocean heat content (Wang et al., 2017), 2) the lower and higher levels of the trophic chain and small pelagic fisheries including tuna and sardines (Ormaza et al., 2016a, 2016b), 3) biogeochemical air-sea CO_2 fluxes (McKinley et al., 2006), 4) the frequency of la Niña/El Niño (Newman et al. 2003). The interactions between decadal oscillations PDO/IPO and AMO may affect also ocean heat content (Chen and Tung, 2014). All these low and high frequency oceanographic events have a direct impact on local, regional and global climate patterns, and there is growing evidence that the driving source of energy is the sun (Grey et al., 2010). Thus, Huo and Xiao (2016) have found a positive strong correlation between El Niño 2015-2016 and SS, as well as SS and the El Niño Modoki index. White et al., (1997) reported that heat anomalies produced by variable solar irradiance are stored in the upper ocean layer, driving SST changes of 0.01-0.03 K and 0.02-0.05 K on decadal and interdecadal periods respectively. Zong et al. (2014) in their review of the impact of the 11-year SS cycle and multidecadal climate projections, have found global SST variations of 0.08 ± 0.06 K and 0.14 ± 0.02 during the 11 and 22 year Hale Cycle, combined with a response lag of 1-2 years in relation to the SS (see also, Kristoufek, 2017). Liu et al. (2015) have reported that effective solar radiation plays a role in the modulation of decadal ENSO (El Niño and the Southern Oscillation) oscillation. More recently, Yamakawa et al. (2016) have reported that solar activities in terms of SS numbers not only affect the troposphere but also the sea surface, even though SS abundance is only a partial measure of solar activity (Scafetta, 2014). The work reported here investigates how sun spots may affect low and high frequency oceanic events such as the Pacific Interdecadal Oscillation (PDO), the Atlantic multidecadal oscillation (AMO), anomalous sea surface temperatures, and El Niño and La Niña events.

Material and methods.

Data for monthly sun spot number (SS) were taken from the Royal Observatory of Belgium, Brussels, World Data Center SILSO (http://www.sidc.be/silso/datafiles). Data sources for other variables were as follow: El Niño regions areas 3.4 (5°North-5°S, 170-120°W) and 1+2 (0-10°S, 90°W-80°W):

- **Sea surface temperatures (SST) and SST Anomaly**: The Monthly Extended Reconstructed Sea Surface Temperature Version 4 (ERSSTv4, 1981-2010 base period). The Optimum Interpolation 1/4 Degree Daily Sea Surface Temperature (OISST.v2, 1981-2010 base period), http://www.cpc.ncep.noaa.gov/data/indices/.
- **Oceanic Niño Index** (ONI: Huang et al., 2014): ERSST.v4 for El Niño/La Niña events since 1950 till December 2017: http://www.cpc.ncep.noaa.gov/products/analysis_monitoring/ensostuff/ensoyears.shtml.
- **Multivariate ENSO index** (MEI: Wolter and Timlin, 2011): https://www.esrl.noaa.gov/psd/enso/mei/table.html.
- **Pacific Decadal Oscillation** (PDO, based on Mantua Index): The PDO index is based on NOAA's extended reconstruction of SSTs (ERSST Version 4). It is constructed by regressing the ERSST Anomaly against the Mantua PDO index for their overlap period, to compute a PDO regression map for the North Pacific ERSST Anomaly. The ERSST Anomaly are then projected onto that map to compute the NCEI index. The PDO index closely follows the Mantua PDO index at: https://www.ncdc.noaa.gov/teleconnections/pdo/ (Wolter and Timlin 1993, 1998 and 2011).
- **Atlantic Multidecadal Oscillation** index: https://www.esrl.noaa.gov/psd/data/timeseries/AMO/.

All indexes have data from April 1954 to December 2017. The analysis was done using Excel and/or R statistical tools. The correlation exercises were executed using SS solar cycles as complete time series against SST Anomaly (in El Niño regions 3.4 and 1+2), ONI, MEI, AMO and PDO indexes. Correlations with lags of 0 to 48 months were carried out. For the SS cycles 19-23 and their impact on the above mentioned dependent variables, correlations were carried out for the whole time series (1954-2017), and for 1990-2016, for each cycle and for their respective ascending and descending phases. Spectral analysis and polynomial regression fitting curves were determined to obtain the slope of the ascending phases; the slopes were correlated to the oceanographic indexes.

Results and discussion:

The time series (1954 to 2016) of SS, PDO, AMO, ONI and MEI are shown in Fig. 1. The PDO, AMO, ONI and MEI cycles have been offset by 0, 12, 24 and 36 months (panels a, b, c and d respectively), whilst the SS series starts at t=0 in the four panels. It has been reported that the lag times for responses of some indexes to SS cycles (SS#) are around 12-36 months (e.g., Zhao et al., 2014). From 1954 to the present time each cycle 19 to 24 has occurred with a period of around 11 years (Hathaway, 2015), which is slightly less than the 11.2 years reported by Dicker (1978). The highest SS activity is seen in cycle 19 with around 250 SS/month, followed by <150, and at cycle 21 around 200, before decreasing steadily over cycles 22 to 24 to just over 100 SS/month. Cycle 24 is the lowest contemporary value of SS activity that is comparable only to cycles 12-15 (around 1880-1930) and is the lowest in the last 200 years (Clette et al., 2014). The negative or cold PDO phases (1947-1976, 2000-June/2016) are within SS cycles 19-20 and 23-24, whilst cycles 21 and 22 are within the positive or warm phase of the PDO (1977-1999). As the PDO and AMO indexes are displaced from 0 to 36 months on the time scale (Fig. 1), some peaks and troughs relative to SS activity can be seen. These are at ascending and descending parts of the SS cycles, e.g. during cycles 19-20 and 23-24 PDO indexes are basically negative, whilst during 21-22 they are more positive; an exception is around 1990, where there is a strong negative peak. However, AMO phases seem to be in opposition to and overlapping the SS cycles; a cold phase of AMO was between the 1960s and 1990s, whilst the warm phase is from the 1990s to the present (McCarthy and Haigh, 2015).

The ONI and MEI curves, both indicators of ENSO events, behave similarly throughout the study period (April 1954 – December 2017). However, MEI has the highest anomaly peaks (> 2) when compared to ONI. In general, ONI and MEI curves indicate the highest positive anomalies between 1978 and 1995, a period that coincides with the warm and cold phases of PDO and AMO respectively (see Maleski and Martinez, 2018). The opposite trend occurs before and after this period due to the inversion of phases. In addition, the highest peaks of both indexes only occur during the ascending and descending phases of the solar cycles; that is, they never coincide directly with the maximum period of sunspots in the cycles, except in 1959. The two highest MEI peaks occur during the descending phase of solar cycle 21 and ascending phase of solar cycle 23. In mid-2016 both indexes increased reaching the third highest peak of this period during the descending phase of SS#24. Negative peaks of these indexes occurred either in the high or low plateaus of the SS curves.

The number (N) of data in the analysis were: 765 (1965-2017); 312 (1990-2016); 108 (1990-1999); 192 (2000-2016). For individual cycles 19 to 24: 127, 141, 124, 117, 141 and 120 respectively. In the same order for ascending-descending phases: 48-80, 50-92, 43-82, 33-85, 51-51 and 74-47. The degrees of freedom of residuals were N-2. The degree of correlation in terms of Pearson coefficient is referred to as: high, moderate and low when the coefficient is between ±0.5 and ±1.0, ±0.3 to ±0.49 and less than ±0.29 respectively (http://www.statisticssolutions.com/pearsons-correlation-coefficient/). All linear regression residuals were auto correlated using the Durbin-Watson (DW) test (Montgomery et al., 2001) for 1954-2017, 1990-2016, 1990-1999, 2000-2016, individual cycles, and ascending-descending phases. The DW test results for the long time series averaged 0.122, for individual cycles it varied from 0.10 to 0.63 with an average of 0.18, and for the ascending and descending phases it averaged 0.40 and varied from 0.1 to 2.24. The SST Anomaly in region ENSO 1+2 has the lowest and PDO the highest.

Whole series (1954-2017) correlations. All variables (Table 1) were correlated on a linear and polynomial (n= 2 to 6th order) basis using different lag times (0, 6, 12, 24 and 48 months) over the six SS cycles. Polynomial correlation (not shown) as well as linear ones displayed poor correlation coefficients, with the highest linear r^2 ($p \leq 0.01$) coefficients occurring at lag times between 12 and 24 months, and 36-48 months for the AMO. For SST and SST Anomaly in ENSO areas 1+2 there was no correlation. These results are like those of Kristoufek (2017), who suggested a surface thermal response of around 24-36 months. The highest correlation r^2 values with SS were up to: 0.043, 0.029, 0.040 and 0.021 for PDO, MEI, ONI and SST Anomaly (in 3.4) respectively, indicating there is a correlation with high confidence (p-value ≤0.01), though small r^2. This fact could reflect sun activity (sun spots) in the long term being balanced by the ups and downs of the cycles. This correlation exercise suggests there is not a good correlation of these indexes in the Pacific and Atlantic over the studied time scale. Nonetheless, on longer time scales, where SS cycles are affected by other sun internal processes, e.g., the hypothesized Minimum of Maunder (Eddy, 1976, Shindell et al., 2001, Ineson et al., 2015, Mörner, 2015, etc.), there can be an impact on a global and regional basis. Recently, Lockwood (2010 and 2013) has reported that a grand solar minimum is coming as the SS cycle 24 is developing. There has not been a solar activity decline such as that found in SS# 23 to 24 over the last 9300 years, and such a solar minimum may last through cycles 24, 25 and 26 (Hady, 2013). Under these circumstances where anomalous conditions appear to be developing, it was decided to analyze correlations using individual cycles in the range 19 to 24.

Period 1990-2016. Further analysis was carried out for the period 1990 to 2016, that includes cycles 22, 23 and 24. The time series was also split into 1990-1999 and 2000-2016, because during 1990-1999 a strong (1991-1992), moderate (1994-1995) and the strongest El Niño (1997-1998) of the twentieth century occurred. On the other hand, in 2000-2016 (cold phase PDO) there were strong La Niña events (2000-2002 and 2010-2012) and an El Niño Modoki event in 2015 (Huo and Xiao, 2016). Figure 2 shows again a poor correlation (<0.011, p>0.246), for the SST Anomaly in region 1+2 (blue bars), although this region was gravely affected by the strong El Niño in 1997-1998 which brought hundreds of casualties and losses of billions of US dollars to the Ecuadorian infrastructure (Glantz, 2001). The linear correlation r^2 of SST in 3.4 (red bars) was around 0.1193 (p≤ 0.00001) over the whole period, whilst it was somewhat higher in the period 1990-1999 (0.1519, p≤ 0.01). The ONI (green bars) correlation coefficient was up to 0.1436 ($p \leq 0.02$) when compared to SS in the period 1990-2000, where high positive SST anomalies were present for almost 6 years, and the ONI correlated better than SST anomaly with SS in 3.4. The Pacific Decadal Oscillation (Fig. 2., grey bars) had an r^2 of 0.276 ($p<0.0001$), in the period 2000-2016 (PDO in a cold phase), with a Pearson correlation of 0.523 that can be considered as high (https://www.statisticssolutions.com/pearsons-correlation-coefficient/). However, for the period 1990-1999 it was 0.239 and for the whole period was 0.402; i.e. a poor and fair degree of correlation respectively.

Individual Cycles. Correlation analysis was split into SS cycles from 19 to 24. The SS and SST r^2 coefficient indicated a poor correlation and confidence level ($p \geq 0.05$) in region 1+2 in all cycles (Fig. 3); most of the correlation r^2 values were <0.050, except in cycle 19, (r^2 of 0.0675, p=0.0032); in cycles 21 and 23 the highest r^2 was 0.046 (p=0.0173) and 0.048 (p=0.037) respectively. In general, the lag time varied between 6 to 36 months in region 3.4, whose correlations r^2 were up to 0.219 ($p \leq 0.0001$) and 0.213 ($p \leq 0.0001$) for cycles 23 and 19 respectively with a lag time of 12-36 months. Cycles 20 and 22 had r^2 of 0.105 ($p \leq 0.0001$) and 0.074 (p=0.003) respectively. The slopes of the linear regression curves with the highest r^2 were positive in region 3.4, indicating a direct correlation between SST and SS cycles. However, cycles 22 and 23 in the region 1+2 exhibited inverse correlation (Fig. 3). Further polynomial correlation (n=2 to 6) analysis did not provide a better r^2. Over all, higher correlations were found in El Niño regions 3.4 than in 1+2.

Anomalies in SST. The magnitude of the SST Anomaly can change depending on the reference used; there are 5 versions of ERRS (Huang et al., 2017). Currently version 5 tends to be used in El Niño studies. Here we used the ERRSv4 (Huang et al., 2014); Huang et al. (2017) stated that there is not a noticeable difference between ERRSv4 and ERRSv5. The anomalies of SST in 3.4 and 1+2 were also correlated against every SS cycle; correlation r^2 values were not better than 0.396 ($p \leq 0.0001$) in both regions, with higher variability in 1+2 than 3.4 both in response time and correlation coefficient (Fig. 4). In region 3.4, the highest correlations were 0.289 ($p \leq 0.0001$) and 0.270 ($p \leq 0.0001$) during cycles 19 and 23 respectively, with a lag time of between 12 and 36 months, with both occurring during cold phases of PDO (1955-1978, and 2000-present). Surface winds plus other oceanographic variables (e.g. upwelling) could play an important role in this high variability. Winds are not only generated in the local area but farther away, including the trade winds of the western Atlantic (Ormaza-González and Cedeño, 2017). Also, ENSO processes in the western Pacific could add variability in the SST Anomaly. The slopes of the linear correlation were basically positive for 3.4 and negative for 1+2, and for SST correlations for cycles 19, 23 and 24 (cold PDO phase) had the highest r^2. Again, the anomalies in 3.4 were better correlated than in region 1+2.

ONI. The El Niño index (Fig. 5) displayed r^2 values when correlated with SS activity from around 0.053 ($p=0.01$, SS# 22) up to 0. 25 ($p << 0.0001$, SS#24); there were poor to fair correlations with a positive slope in SS cycles 19, 23 and 24. During SS# 24, ONI reached extreme values of 2.6C (Nov-Dec-Jan 2015/2016) and -1.7C (Oct-Nov-Dec 2010). The highest r^2 were again found with a 24-48 months lag time. Cycle 21 did not show any significant correlation with ONI; however, cycles 20, 22 and 24 had r^2 values of 0.144 ($p<<0.001$), 0.131 ($p<<0.0001$) and 0.252 ($p<<0.0001$) and lag times of 48, 12, and 24 months respectively. Recently, Huo and Xiao (2016) found strong correlation between SS and El Niño Modoki during 2015 (SS#24). The variability in correlations could arise from: 1) SS numbers showing large variations from one month to another, 2) regional meteorological conditions (particularly cloudiness), ocean surface currents that exchanges heat in region 3.4, 3) Kelvin waves (Gill, 1982), 4) the Southern Oscillation Index (SOI: Southern Oscillation Index: http://www.cpc.ncep.noaa.gov/data/indices/soi). All these may affect the SSTs and together with the way ONI is obtained, as the ONI has a variable reference period of 30 years; thus for 1950 to 1955 the reference period is 1936-1965; for 1956-1960; 1941-1970. The ERRSv4 uses the period

1981-2010. The reference period is changed every 5 years (Lindsey, 2013); the most recent ONIs (v4/v5) are supposed to use better and more consistent information as data acquisition improves.

MEI. This additional index for El Niño events had a lower correlation (r^2) with SS; thus, the highest value was 0.3943 (p<<0.00101, SS# 19), the next 0.3028 (p<<0.00001, SS#24), 0.2421 (p<<0.00001, SS# 23) and 0.1566 (p<<0.0001, SS# 20); in cycles 21 and 22 no correlation better than 0.1232 (p<<0.0001) was found. The lag time for sun spot activity (with the highest correlations) ranges from 24-48 months; and linear regression curves were with mainly positive slopes. The lower correlation found could be explained as this index comprehend six variables, and some of these could not be directly or are weakly related to SS; like zonal and meridional components of surface wind, surface air temperature, cloudiness (Wolter and Timlin, 1993).

PDO. This interdecadal index (Fig. 5) is linearly correlated to SS cycles with a lag time between 36 and 48 months, with the highest r^2 of 0.391 (p<<0.00001) in cycle 19, and 0.586 (p<<0.00001) for cycle 24. Both cycles are within the cold phase of the PDO. The next highest r^2 with p-values <<0.0001 were 0.218, 0.1361, 0.218 and 0.260 for cycles 20-23. In all cycles, the highest r^2 were directly correlated, except cycle 20. For some reason, there appears a better fit with both PDO and ONI in cycles 19 and 24, which are within the cold phase of the PDO, even though these cycles have remarkably different shapes and peaks (Fig. 12). Cycle 19 registered SS counts of over 250 whilst cycle 24 was just around 100; also, the peaks were different being respectively very sharp and extended. The direct relationship between PDO and ONI has been reported extensively (e.g. Ormaza-Gonzalez et al., 2016 a, Jia and Ge, 2017).

AMO. This index gave correlation coefficients (r^2) with SS numbers of up to 0.490 (p<<0.00001) and down to 0.162 (p=0.0004) in cycles 20 and 24 respectively, when a lag time of 48 months was used.

With cycles 19, 21 and 22 the best fit elapsed time was 24-36 months. Gray et al. (2016) reported lag time responses of mean-sea-level pressure over the Atlantic to SS cycles of 36-48 months over a longer time series study of 32 solar cycles. Figure 6 shows the bar distribution of the r^2; it displays linear regression with positive and negative slopes for cycles 19, 23 and 24; and 20 to 22, respectively. This coincides with the phases of the AMO, negative from around 1965 to 1998 (SS cycles 20-22), and positive; 1930-1965 (SS cycle 19) and after 1998 (SS cycles 23-24), http://appinsys.com/globalwarming/amo.htm . It is noteworthy that the slopes of the PDO and AMO linear regressions are negative and positive respectively for cycles 21 and 22, but in concordance in cycles 19, 20, 23 and 24 (cold phase PDO).

Ascending and descending phases of solar cycles. As the SS cycles are best related to variables studied on a response time from 24 to 36 months, there was the need to study their influence during the ascending and descending phases, which have roughly 5-6 years duration. Polynomial regression analysis was performed to establish a function that could best describe every SS cycle. Sixth-order polynomial curves (Fig. 12) were found to render a very strong correlation coefficient averaging 0.89 ($p \leq 0.001$). These functions allowed the analysis of correlations in the ascending and descending phases.

SST in 1+2 and 3.4. In region 1+2, the highest correlation coefficient r^2 and p-value were, respectively, 0.205 and 0.0008 (SS# 23), 0.189 and ≤0.0036 (SS# 21), and 0.163 and ≤0.0044 (SS# 19). All linear regression coefficients r^2 over 0.0847 ($p<0.05$ to $=0.0008$) occurred in the ascending phase of the SS cycles, whilst those in the descending phase were lower, with no definite lag time pattern from 0 to 36 months. The slope (positive/negative) of the linear regression (Fig. 7) curves showed no pattern. These low and variable r^2 values reflect region 1+2 being subjected to the combined impact of many diurnal and seasonal oceanographic and meteorological variables. For example, during the first quarter of 2017 (cycle 24), in 1+2 there was a higher than usual SST because the southern trade winds in the eastern Pacific weakened whilst those in the North Atlantic strengthened. These winds passed through the Panama Isthmus and blew warm (up to 30C) surface waters from the Panama Bay southwards towards area 1+2, thus provoking a rapid and relatively short lived surface warming event (Ormaza-González and Cedeño, 2017), whilst region 3.4 was registering La Niña conditions. This cold event also strengthens the Cromwell Undercurrent (Knauss, 1959) and Humboldt (Montecino and Lange, 2009) currents that impact upwelling processes in 1+2. During the ascending phases of the cycles, the correlation of SSTs was higher than in the descending phase of cycles. All these factors would mask the SS signal in this area.

In the region 3.4, the maximum r^2 of SST in each SS cycle was found at a lag time of 36 months with all of them occurring at the ascending phase, except in cycles 20 and 24. The four highest r^2 values were 0.870 (p=0.021, SS# 24), 0.613 (<<0.0001, SS# 22), 0.574 (p<<0.0001, SS# 19), and 0.556 (p<<0.0001, SS# 23) with Pearson coefficients of 0.9327, 0.7803, 0.7576 and 0.7456, respectively, thus showing a strong degree of linear correlation. Linear regression slopes were variable (Fig. 7), although there was a tendency in cycles 20, 21 and 22 (warm PDO) for negative slopes and for positive slopes for cycles 19, 23 and 24 (cold phase PDO). In area 3.4 the SST response to SS was much clearer than for 1+2, as in this region (10N-10S and 120W-180W) there is no influence of coastal processes. The highest r^2 (0.870, p=0.021; lag time 36 months) in the descending phase in cycle 24 coincided with the strongest El Niño, and the second-highest r^2 (0.613, p<<0.00001) during ascending phase of cycle 22 with two consecutive strong El Niño 1991-1995; the third r^2 (0.574, p<<0.00001) during cycle 19, with el Niño 1955-1957, and finally the fourth r^2 (0.556, p<<0.00001) with the 1997-1998 warm event during cycle 23. It seems that over the relatively short time scales of SS cycles, either on their initial ascending or subsequent descending phases, impacts on the SSTs can be triggered.

SST Anomaly. In region 1+2 (Fig. 8), the anomalies registered high r^2 ($p<<0.0001$) of 0.662 (SS# 22), 0.637 (SS# 19), 0.523 (SS# 21), 0.480 (SS# 23), 0.359 (SS# 24); and 0.254 ($p=0.0002$, SS# 20) respectively, in the ascending phase of the SS cycles and with a positive linear regression slope (except SS# 23). The response lag time was somewhere between 0 and 48 months. On the other hand, the descending phase showed a predominantly lower r^2, less than 0.14 with lower significance ($p \leq 0.02$), with the exception in SS# 19, 0.304 ($p<<0.0001$). The results suggest that during cold phase PDOs when Northern Pacific basin surface ocean waters are relatively colder, the correlations in this area tend to be higher, as the increasing sun radiation augments the heat content (SST) of the ocean surface.

In region 3.4, there was a high and consistent r^2 (Fig. 8) that reached up to 0.897 ($p=0.014$; SS# 24); 0.863 ($p<<0.0001$; SS# 22); 0.665 ($p<<0.0001$; SS# 19), 0.826 ($p<<0.0001$; SS# 23), then fell to 0.211 ($p=0.008$; SS# 20); 0.239 ($p=0.0009$; SS# 21) respectively; all of them were in the ascending phase except cycles 20 and 24. The lag time was consistent at 36 months. Linear regression slopes were variable (Fig. 8) with negative slopes in cycles 20-22 (warm phase PDO), and positive slopes in 19, 23 and 24 cycles (cold phase PDO). The highest r^2 of 0.897 at the start of the descending phase in 24 coincided with one of the strongest El Niño and the second r^2 (SS# 22 ascending phase) with two consecutive strong El Niño 1991-1995. The third and fourth highest r^2 were during El Niño 1955-1957 and 1997-1998 warm event (SS# 23 ascending) respectively. The results suggest that SS cycles are strongly correlated to SST Anomalies in both El Niño regions, with the strongest relationship in 3.4.

The ONI index. This index as well as SST and its anomalies in 3.4, were equally strongly associated with the ascending phase of the SS cycles (Fig. 9), with lag times of 24-36 months. The highest correlation r^2 for each cycle were in the ascending phase, the predominant linear regression slopes were positive, except for SS# 20. The highest r^2 ($p<<0.0001$) were: 0.817 (SS# 22), 0.693 (SS# 19), 0.637 (SS# 23), 0.3547 (SS# 24), 0.2876 (SS# 20); 0.1936 ($p=0.003$, SS# 21). The three highest r^2 match the dates of full-fledged strong El Niño 1955-1957, 1987-1989, and 1997-1998 (Fig. 9) with positive slopes on the ascending phase. In the descending phase the r^2 ($p<<0.0001$) in cycles 24, 23, 22 and 20 were 0.366, 0.284, 0.255, and 0.242 respectively. All had a lag time 0-12 months and positive slopes. Cycles 19 and 21 showed neither strong correlation (<0.1) or confidence values ($p=0.2$). The ONI correlations are in accordance to what found with SST anomalies in 3.4.

Warm events tend to occur in both ascending/descending phases after the peak/trough, and have a delay time of 36 months, which is similar to findings of Huo and Xiao (2016). The delay time, is probably due to the slow accumulation of solar heat over time in surface oceanic waters. The descending phase of the cycles (Fig. 9), with a smaller slope than the ascending phase, produces a quicker response (0-12 months) to the ocean surface SST and ONI that could trigger neutral or cold events more cogently. Most of the la Niña events occur during the descending phase or approaching the cycle minimum (Fig. 10), when the solar irradiance (SI) decreases slightly as does the number of sunspots. The weakest sunspot cycle (SS# 24) has had three La Niña events: 2007-2009, 2010-2012, 2016-2017 (Fig, 12). A plausible reason is that during this cycle the number of sun spots (i.e. sun activity) is the lowest in the last two centennials (Clette et al., 2014); therefore, less energy has hit the ocean surface allowing a cooling effect. Two important exceptions are La Niña 1988-1989 (22) and 2000-2002 (cycle 23) that occurred in the ascending phase.

The MEI index. The Multivariate ENSO Index does not only consider the SST Anomaly but also sea-level pressure (Allan and Ansell, 2006) and other variables. These variables include surface winds (meridional and zonal), surface air temperature and cloudiness (Wolter and Timlin, 1998). The MEI correlated at slightly lower levels with SS cycles with r^2: 0.784 ($p \leq 0.0001$), 0.770 ($p<<0.0001$), 0.5972 ($p \leq 0.0001$); 0.3396 ($p \leq 0.0001$); 0.2368 ($p=0.0003$); and 0.222 ($p=0.001$) for SS cycles 19, 22, 23, 24, 20, and 21, respectively. All of them were in the ascending phase of the cycles with lag times from 12 to 48 months (except cycles 23 and 24), with a positive linear regression slope. Exceptions were 22 and 20 where the r^2 was largest with a zero lag time. During the descending phase, as with the ONI, the r^2 were lower: 0.321 ($p=0.0004$, SS# 24); 0.3145 ($p<<0.0001$, SS# 19); 0.2234 ($p<<0.0001$, SS# 22); 0.2088 ($p<<0.0001$, SS# 20), and 0.1438 ($p=0.0002$, SS# 23) with positive slopes (except SS# 20), and lag times predominantly in the 0-48 month range; cycle 21 did not have a r^2 above 0.010 ($p>0.02$). For the MEI index, as with ONI, the r^2 were much lower during descending phases, when there is less sun radiation energy (see formula 1), thus La Niña events could be expected as it actually has occurred in the six cycles. The lower correlations could be because the MEI uses five variables more than the ONI, and these could thus help obscure the signal from the sun's irradiation.

PDO. The Pacific Decadal oscillation gave positive linear correlations and slopes with SS in most cycles except cycles 20 and 21. Correlation coefficients of 0.7677 ($p \leq 10^{-12}$), 06577 ($p \leq 10^{-12}$), 0.6734 ($p \leq 10^{-7}$) and 0.5062 ($p \leq 10^{-7}$) for the ascending phase SS# 19 (Apr/54-Nov/58), SS# 24 (Jan/08-Feb/14), SS# 22 (Sep/86-Jan/89) and SS# 23 (May/90-Jun/00) respectively were found. All these coefficients were obtained at a lag time of 12-48 months, except 22 and 23 (t=0). The slopes of the linear regressions were mainly positive during cold phase PDOs (cycles 19, 23 and 24), except cycle 20 when a cold PDO was transitioning to a warm PDO (cycles 21 and 22). Figure 10 shows that linear correlations in cycles 19, 21, 23 and 24 showed positive slopes. The two highest r^2 values are at a lag time of 12-36 months, for cycles 19 and 24, as has been reported (e.g., Huo and Xiao, 2017). During the descending phase, the correlation r^2 tended to be much lower, with the highest 0.3522 ($p<<0.00001$) and 0.3452 ($p<<0.00001$) at cycles 19 and 20. Sun spot energy variations on long time scales (van Loon et al. 2007), even with very weak changes, could produce decadal and millennial timescale impacts on global thermohaline circulation that in turn affect heat distribution (Bond et al. 2001, Gray et al., 2013).

AMO. The correlations were generally higher at the descending phase of the SS cycles (Fig. 11), which is opposite to those for SS vs PDO, ONI, MEI, and the SST Anomaly. However, the highest r^2 occurred on ascending (A) and descending (D) phases of SS cycles, thus: 0.700 ($p \ll 10^{-10}$), 0.558 ($p \ll 10^{-10}$), 0.468 ($p \ll 10^{-10}$), 0.434 ($p=0.03$), 0.411 ($p \ll 0.00001$) and 0.191 ($p=0.001$) for cycles 20A, 22D, 19D, 24D, 21A and 23A, respectively. These high r^2 values show a strong degree of correlation, although lower than PDO correlations. The lag time was between 24-48 months. The results found could be explained as The Atlantic Multidecadal Oscillation index has the opposite phase to the PDO (Enfield et al., 2001; Condron et al., 2005); i.e. warm in periods 1930-1964 and 2000-present (cold PDO), and cold in 1965-1999 (warm PDO).

Conclusions

Period 1954-2017. Over this period sun spot numbers have decreased from between 225 (SS# 21) and 110 (SS# 24) at cycle maxima, to minima SS counts of around 20-25. Thus, the Earth is receiving decreasing solar energy over this almost 7-decade period. The reduction of SS peaks has been associated with the beginning of the Maunder Minimum (Mörner, 2015). Ineson et al. (2014) are projecting lower peaks for the next SS cycle (SS# 25) and presently SS counts per month are as low as 1.6 (July 2018) and with an average of 8.5 (Jan-Aug 2018); counts are expected to decrease to 5.3 in February 2019, actually it decreased to 0.8 (http://www.sws.bom.gov.au/Solar/1/6)

Monthly SS count correlations with SST, SST Anomaly (both 3.4 and 1+2), ONI, MEI, AMO and PDO through the whole time series (1954-2017) were poor; these had a correlation r^2 values averaging 0.020 and a negative linear regression slope. Thus, in the long term there are no strong correlations between SS and PDO, MEI, ONI and SST Anomaly in 3.4 (correlation coefficients were between 0.043 and 0.021). In the case of region 1+2, the correlation was even poorer: <0.005.

The series of correlations at different lag times (6, 12, 24, 36 and 48 months) gave a response time (i.e. the lag time with highest correlation coefficients; Table 1) of 12-24 months for all indexes, except for AMO (48 months), which align to what was previously reported by Kristoufek, (2017), and Huo and Xiao (2016);

Changes of the SS cycle could have climate impacts. Gil-Alana et al. (2014) have found no significant statistical relation between sun spots and global temperature; however, van Loon et al. (2007) suggested that even though SS cycles produce weak changes on Solar Irradiation (SI) of about 0.07% according to Gray et al. (2010), these can still produce decadal and millennial impacts on global thermohaline circulation (Bond et al. 2001, Gray et al., 2016), due chiefly to UV energy fluctuation (Ineson et al., 2014). The changes in UV (<100 nm to 350 nm) and near infrared (>800 nm to >1000 nm) are larger than in the visible range (>350 nm-800 nm) and could have an important impact on global climate (Ermelo et al. 2013). It is therefore reasonable to expect some impact on the studied oceanographic indexes. Recent data (Solar Radiation and Climate Experiment Satellite) suggest that the variability of UV radiation during the declining phase of cycle 23 was larger than previous estimates (Harder et al., 2009 and Haigh et al., 2010). The SI variations are strongly correlated to SS, and even though these are relatively small (Hansen et al., 2013), they may impact surface ocean heat content because: 1) the total SI integrates over all the wavelengths, and 2) the heat capacity of the seawater is huge. Also, UV radiation penetrates down to 75-100 m depth in the water column (Smyth, 2011), thus adding to the heat content of the deeper layers.

Individual SS cycles (19-24). The SST shows some correlations against individual SS cycles in regions 3.4 and 1+2. In the first (Fig. 3), these were up to 0.219 (SS# 23) whilst the lag time was 12-36 months in all cycles (except SS# 19), in line with reports from Kristoufek (2017) and Huo and Xiao (2016). On the other hand, in region 1+2, the linear correlation r^2 was low at <0.0675 (SS# 19), and highly inconstant between cycles. The SS and SST anomaly correlations in 3.4 and 1+2 (Fig. 4), showed important variability with highest values of 0.289 (in 3.4) and 0.396 (in 1+2) during cycles 19 and 24 respectively, with both having the same response time range. These values are within the cold phase of the PDO, suggesting that during this phase the signal from SS is clearer. In the period 1997-2016 the two strongest El Niño (1997-1998 and 2015) and La Niña (2000-2002 and 2010-2012), events occurred, and they were most evident in the 1+2 region. The slopes of the linear correlation were positive for 3.4 and negative for 1+2, and in general it was found that correlations were more inconstant and lower in 1+2 than in 3.4. These results do suggest that Sun spot activity can influence the SST and SST anomaly behavior, but the relatively weak signals may well reflect high seasonal and interannual variability in coastal oceanographic conditions (Ormaza-González and Cedeño, 2017) that obscures the correlation with SS. In zone 3.4, correlations are better, although the influence of regional oceanographic and meteorological conditions will still be there as expressed through, e.g., the Southern Oscillation Index (Rasmussen and Carpenter, 1982; Barnston, 2015). During cycle 24, the ONI index was highly correlated to SS (r^2 up to 0.2510) with a positive slope (Fig. 5). The ONI index reached 2.6C (Nov-Dec-Jan 2015/2016) and -1.7C (Oct-Nov-Dec 2010). In cycles 20-21 the r^2 was low (r^2<0.04); however, from 22 to 24, r^2 increased from 0.131 (p<<0.00006) to 0.251; thus, confirming the SS activity has a better correlation during the cold phase of PDO.

The PDO aligned best with SS cycles at lag times of 36-48 months during SS#19 (0.625) and SS#24 (0.766) when the PDO was in a cold phase, whilst lower correlations (0.467-0.508 for cycles 20-23) were found when it is in a warm phase (1979-2000) or in between them. The North Atlantic index counterpart, the AMO index, gave a variable correlation r^2 ranged from 0.130 to 0.490 with a response time of 48 months for cycles 23 and 20 respectively. Gray et al. (2016) reported 36-48 months lag for mean-sea-level pressure in the North Atlantic in a study of 32 SS cycles. The slopes of the PDO and AMO linear regression curves are negative and positive respectively in cycle 21 and 22, but in concordance in 19, 20, 23 and 24 during the cold phase of the PDO. These two interdecadal oscillations proved to be correlated to SS, with the PDO having a higher correlation. Presumably, as the North Pacific Ocean basin has a larger area than the North Atlantic the correlations and lag times may reflect the higher heat storage capacity in the North Pacific.

Ascending and descending phases. The SSTs in 1+2 showed higher correlations with SS in the ascending phases, relative to the descending phase (r^2 of up to 0.205 and below 0.067 respectively). In region 3.4, there were again high degrees of correlation of SS and SST (r^2 between 0.87 and 0.56), during the ascending phase of the cycles, with a response time of 36 months. The highest r^2 of 0.870

in the descending phase in cycle 24 coincided with the strongest El Niño (2015) and the second highest (SS# 22) with two consecutive strong El Niño events in 1991-1995; the third and fourth highest corresponded with el Niño and warm events respectively in 1955-1957 and 1997-1998. It seems that short time expressions of SS cycles, either at the beginning of their ascending or descending phases, have a trigger effect on the SSTs. This was observed through the polynomial regression curves (Fig. 12) that were found for each SS cycle, as the SI (equation 1) increases and decreases the amount of heating of surface waters follows suit. The polynomial curves (6^{th} order) were fitted with an average r^2>0.89. However, a response time of 24-36 months seems to occur at the low or high plateau of the cycles (Fig. 12). Thus, the warm events El Niño of: 1957-1958 (SS# 19), 1965-1966 (SS# 20), 1981-1982 (SS# 21), 1987-1988 and 1991-1992 (SS# 22), 1997-1998 (SS# 23), 2015-2016 (SS# 24). On the other hand, the cold events of La Niña tend to occur after an El Niño at the middle of the ascending phases (1988-1989, 1999-2001, 2010-2012) or when approaching the minimum of the cycles (1973-1974, 1975-1975; 1995-1996, 2017-2018). The so called equatorial Pacific neutral conditions in 3.4 (see, https://iridl.ldeo.columbia.edu/maproom/ENSO/ENSO_Info.html), seems to span a longer period after La Niña, and vice versa after El Niño.

The ENSO indexes ONI and MEI also showed strong correlations to the ascending phase of the SS cycles, with a lag time of 24-36 months. In this analysis, it was also found that warm events tend to occur in the ascending phase (SI increases) or at the top of the cycle and have a delay time of 36 months (as also reported by Huo and Xiao, 2016), whilst cold events are mostly associated with a descending phase (SI decrease) but with a quicker response time of 0-12 months. During the descending phase, the correlation coefficients were lower and variable with positive slopes and shorter lag times of 0-12 months. The MEI index has a similar pattern to the ONI, but with lower correlations that may arise as the MEI takes into consideration six variables that in combination may mask the signal from sun activity.

The PDO (Fig 10) was linearly correlated to SS (r^2 ranging from 0.285 to 0.768) in the ascending phase with lag times of 24-36 months (Huo and Xiao, 2016), whilst correlations with AMO (Fig. 11) varied with r^2 between 0.160 to 0.700. Similarly, the response time was 24-48 months. These results correspond with those of van Loon et al. (2007), who established that even a small change (1.5 W m^{-2}) in sun activity (SI) could produce decadal and millennial time scales influences on thermohaline circulation (Bond et al. 2001, Gray et al., 2016); nonetheless the Intergovernmental Panel on Climate Change: IPPC (2001) considers this fact too small to drive climate changes. These influences of this change can be reflected by PDO and AMO indexes, which are found to be in the opposite phase to PDO (Enfield et al., 2001; Condron et al., 2005). The ascending and descending phases of SS could re-inforce and weaken these indexes.

Recent predictions for an El Niño event in the late northern hemisphere summer of 2018 (see: http://www.bom.gov.au/climate/enso/) did not occur; then, projections were pushed back to the beginning of autumn (http://www.cpc.ncep.noaa.gov/products/precip/CWlink/MJO/enso.shtml) and most recently late autumn and winter. Thus, most current models are failing to provide a consistent projection. This is likely related to two re-cooling events in all El Niño areas, that have kept the ONI index within the realm of ENSO neutrality (-0.5C to 0.5C). Also, the PDO indexes have been negative, averaging -0.53, and it is now in its cold phase (https://www.ncdc.noaa.gov/teleconnections/pdo/). During 2017 the average smoothed SS counts per month was 21.8, and for 2018 it was 8.5 with many weeks without any SS. In July the average SS count was just 1.6 (http://www.sws.bom.gov.au/Solar/1/6) with counts expected to decrease to 5.3 in February 2019 (actually they were just 0.8). Therefore, the input of solar heat has been at its lowest values since the 1950s, and its trigger effect on ENSO system is not enough for a full-fledge El

Niño event. At the time of writing this paper, the expected and modelled 2018 full-fledged El Niño 2018 did not occur, it did not happen, actually the region 3.4 and 1+2 cooled down by the end of 2018. During March 2019, the latest report from http://www.bom.gov.au/climate/enso/#tabs=Overview is saying "The El Niño–Southern Oscillation (ENSO) remains neutral. However, the Bureau's *ENSO Outlook* remains at El Niño WATCH, meaning there is approximately a 50% chance of El Niño developing during the southern hemisphere autumn or winter…". Nonetheless, NOAA view is that a weak El Niño conditions are present now and to expect to continue through the Northern Hemisphere spring 2019 (~55% chance), https://www.cpc.ncep.noaa.gov/products/analysis_monitoring/lanina/enso_evolution-status-fcsts-web.pdf. The fact is, El Niño is not fully-fledged; *id est,* the meteorological (SOI) and oceanographic are not connected. At this moment (march 24, 2019) the oceanographic and meteorological variables have not fully couple yet.

The ENSO modellers should take into account in some way the presence of SS or any variable that could measure the variability of SI as an input to the models, specially the determinists ones.

Data availability. All data are publicly available on the Web (see Material and Methods).

Author contributions. Franklin Isaac Ormaza-González led and oversaw the whole project. He conceptualized the hypothesis, researched the literature, designed the material and methods, and wrote the paper in all its stages. María Esther Espinoza-Celi looked for and retrieved all data and information, run statistical and spectral analysis, organized results, and designed graphs. She designed the poster presentation.

Acknowledgements. Authors are grateful to ESPOL authorities whose supported research allotting time and financial resources to present paper in the "4TH INTERNATIONAL SYMPOSIUM: THE CLIMATE CHANGE EFFECTS ON THE WORLD OCEANS" held in Washington DC, 4-8 June 2018, also The National Chamber of Fisheries of Ecuador support is acknowledged. Work on the English by Dafne Vera-Mosquera and anonymous scientist is indeed appreciated.

References

1. Allan, R.J., and Ansell, T.: A new globally complete monthly historical gridded mean sea level pressure dataset (HadSLP2): 1850-2004, J. Climate, 19, 5816-5842, 2006.
2. Barnston, A.: Why are there so many ENSO indexes, instead of just one? https://www.climate.gov/news-features/blogs/enso/why-are-there-so-many-enso-indexes-instead-just-one (last access: 15 March 2018), 2015.
3. Bond, G. G., Kromer, B., Beer, J., Muscheler, R., Evans, M., Showers, W., Hoffmann, S., Lotti-Bond, R., Hajdas, I., and Bonani, G.: Persistent Solar Influence on North Atlantic Climate During the Holocene, Science, 294, 2130–2136, 2001.
4. Bhowmik, P. and Nandy, D.: Prediction of the strength and timing of sunspot cycle 25 reveal decadal-scale space environmental conditions. NATURE COMMUNICATIONS (2018) 9:5209. https://doi.org/10.1038/s41467-018-07690-0.
5. Busalacchi, A.J., Takeuchi, K., and O'Brien, J.J.: Interannual variability of the equatorial Pacific-revisited, J. Geophys. Res., 88, 7551-7562, 1983.
6. Chen, X., and Tung, K.K.: Varying planetary heat sink led to global-warming slowdown and acceleration, Science, 345, 897–903, doi:10.1126/science.1254937, 2014.

~~7.~~ Clette, F., Svalgaard, L., Vaquero, J. M., and Cliver, E. W.: Revisiting the Sunspot Number, Space Sci. Rev., 186, 35-103, doi: 10.1007/s11214-014-0074-2, 2014.

8. Clutz, R.: Global ocean cooling in September (2017), https://rclutz.wordpress.com/2017/10/26/global-ocean-cooling-in-september/ (last access: 30 October 2017), 2017.
9. Compo, G.P., and Sardeshmukh, P.D.: Oceanic influences on recent continental warming, Clim. Dynam., 32, 333-342, doi:10.1007/s00382-008-0448-9, 2009.
10. Condron, A., DeConto, R., Bradley, R. S., and Juanes, F.: Multidecadal North Atlantic climate variability and its effect on North American salmon abundance, J. Geophys. Res. Lett., 32L23703, doi:10.1029/2005GL024239, 2005.

11. Dicke, R.H.: Is there a chronometer hidden deep in the Sun? Nature, 276, 676-680, 1978.
12. Eddy, J. A.: The Maunder Minimum, Science, 192 (4245), 1189–1202, doi:10.1126/science.192.4245.1189, 1976.
13. Enfield, D.B., Mestas-Nuñez, A.M., and Trimble, P.J.: The Atlantic multidecadal oscillation and its relation to rainfall and river flows in the continental US, J. Geophys. Res. Lett., 28, 2077–2080, doi:10.1029/2000GL012745, 2001.
14. Ermolli, I., Matthes, K., Dudok de Wit, T., Krivova, N. A., Tourpali, K., Weber, M., Unruh, Y. C., Gray, L., Langematz, U., Pilewskie, P., Rozanov, E., Schmutz, W., Shapiro, A., Solanki, S. K., and Woods, T.N.: Recent variability of the solar spectral irradiance and its impact on climate modelling, Atmos. Chem. Phys., 13, 3945-3977, doi:10.5194/acp-13-3945-2013, 2013.
15. Fasullo, J., and Nerem, R.: Interannual variability in global mean sea level estimated from the CESM Large and last millennium ensembles, Water, 8, 491, doi:10.3390/w8110491, 2016.
16. Fröhlich C.: Solar Constant and Total Solar Irradiance Variations, edited by: Richter, C., Lincot, D., Gueymard C.A., Solar Energy, Springer, New York, NY, 2013.
17. Gil, L.A., Yaya, O.S., and Shittu, O.I.: Global temperatures and sunspot numbers. Are they related? Physica A., 396, 42–50, 2014.
18. Gill, A. E.: Atmosphere–Ocean Dynamics, International Geophysics Series, Academic Press, edited by: Donn, W. L., 30, 662 pp., eBook ISBN: 9780080570525, Paperback ISBN: 9780122835223, 1982.
19. Glantz, M. H.: Once burned, twice shy? Lessons learned from the 1997-1998 El Niño, The Unite Nations University, 294 pp, 2001.
20. Gray, L. J., Beer, J., Geller, M., Haigh, J. D., Lockwood, M., Matthes, K., Cubasch, U., Fleitmann, D., Harrison, G., Hood, L., Luterbacher, J., Meehl, G. A., Shindell, D., van Geel, B., and White, W.: Solar influences on climate, Rev. Geophys., 48, RG4001, doi:10.1029/2009RG000282, 2010.

21. Gray, L. J., Woollings, T. J., Andrews, M., and Knight, J.: Eleven-year solar cycle signal in the NAO and Atlantic/European blocking, Q. J. Roy. Meteor. Soc., 142, 1890–1903, doi:10.1002/qj.2782, 2016.
22. Hady, Ahmed A.: Deep solar minimum and global climate changes. J. Advanced Res (ISSN: 2090-1232), Vol: 4, Issue: 3, Page: 209-214. 2013 https://doi.org/10.1016/j.jare.2012.11.001.
23. Haigh, J. D., Winning, A.R., Toumi, R., and Harder, J. W.: An influence of solar spectral variations on radiative forcing of climate, Nature, 467, 696–699, 2010.
24. Harder, J. W., Fontenla, J. M., Pilewskie, P., Richard, E. C., and Woods, T. N.: Trends in solar spectral irradiance variability in the visible and infrared, J. Geophys. Res. Lett., 36L07801, 2009.
25. Hathaway, D. H.: The Solar Cycle, Living Rev. Sol. Phys., 12, 4, doi:10.1007/lrsp-2015-4, 2015.
26. Hansen J, Kharecha P, Sato M, Masson-Delmotte V, Ackerman F, et al. (2013) Assessing ''Dangerous Climate Change'': Required Reduction of Carbon Emissions to Protect Young People, Future Generations and Nature. PLoS ONE 8(12): e81648. doi:10.1371/journal.pone.0081648
27. Henley, B.J., Gergis, J., Karoly, D.J., Power, S., Kennedy, J., and Folland, C.K.: A Tripole Index for the Interdecadal Pacific Oscillation, Clim. Dynam., 45, 3077, doi:10.1007/s00382-015-2525-1, 2015.
28. Horning, N., Russell, C., and Goetz, S.: Energy from the Sun to Earth's Surface. In Chapter 2: Earth's Radiation Balance and the Global Greenhouse, https://people.ucsc.edu/~mdmccar/migrated/ocea80b/public/lectures/lect_notes_1/03_Energy_Balance_MDM_11F.pdf (last access: 25 April 2018), 2003.
29. Huang, B., Banzon, V.F., Freeman, E., Lawrimore, J., Liu, W., Peterson, T.C., Smith, T.M., Thorne, P. W., Woodruff, S. D., and Zhang, H. M.: Extended Reconstructed Sea Surface Temperature version 4 (ERSST.v4): Part I. Upgrades and intercomparisons, J. Climate, 28, 911–930, doi:10.1175/JCLI-D-14-00006, 2014.

30. Huang, B., Thorne, P.W., Banzon, V.F., Boyer, T., Chepurin, G., Lawrimore, J.H., Menne, M.J., Smith, T. M, Vose, R. S., and Zhang, H. M.: Extended Reconstructed Sea Surface Temperature, Version 5 (ERSSTv5): Upgrades, Validations, and Intercomparisons, J. Climate, 30, 8179–8205, doi:10.1175/JCLI-D-16-0836.1, 2017.
31. Huo, W.J., and Xiao, Z.N.: The impact of solar activity on the 2015/16 El Niño event, Atmospheric and Oceanic Science Letters, doi: 10.1080/16742834.2016.1231567, 2016.
32. Ineson, S., Maycock, A. C., Gray, L. J., Scaife, A. A., Dunstone, N. J., Harder, J. W., Knight, J. R., Lockwood, M., Manners, J. C., and Wood, R. A.: Regional climate impacts of a possible future grand solar minimum, Nat. Commun., 6, 7535, doi:10.1038/ncomms8535, 2015.
33. Intergovernmental Panel on Climate Change (IPCC) (2001), Third Assessment Report–Climate Change 2001, The Scientific Basis, Cambridge Univ. Press, New York.
34. Jia, X. and Ge, J. (2017), Modulation of the PDO to the relationship between moderate ENSO events and the winter climate over North America. Int. J. Climatol, 37: 4275-4287. doi:10.1002/joc.5083
35. Knauss, J. A.: Measurements of the Cromwell current, Deep-Sea Res., 6, 265-286, doi.org/10.1016/0146-6313(59)90086-3, 1959.
36. Kopp, G., and Lean, J. L.: A new, lower value of total solar irradiance: Evidence and climate significance, J. Geophys. Res. Lett., 38L01706, doi:10.1029/2010GL045777, 2011.
37. Kristoufek, L.: Has global warming modified the relationship between sun spot numbers and global temperatures? Physica A., 468, 351-358, doi: 10.1016/j.physa.2016.10.089, 2017.
38. Labitzke, K., Austin, J., Butchart, N., Knight J., Takahashi, M., Nakamoto, M., Nagashima, T., Dorothy, J., and Williams, V.: The global signal of the 11-year solar cycle in the stratosphere: Observations and model results, J. Atmos. Terr. Phys., 64, 203-210, doi:10.1016/S1364-6826(01)00084-0, 2002.

39. Lindsey, R.: Climate and Earth's Energy Budget. In NASA Earth Observatory, https://earthobservatory.nasa.gov/Features/EnergyBalance/ (last access: 25 April 2018), 2009.
40. Lindsey, R.: In Watching for El Niño and La Niña, NOAA Adapts to Global Warming, https://www.climate.gov/news-features/understanding-climate/watching-el-ni%C3%B1o-and-la-ni%C3%B1a-noaa-adapts-global-warming (last access: 25 April 2018), 2013.
41. Liu, F., Chai, J., Huang, G., Liu, J., and Chen, Z.: Modulation of decadal ENSO-like variation by effective solar radiation, Dynam. Atmos. Oceans, 72, 52-61, ISSN: 0377-0265, 2015.
42. Lockwood, M.: Solar change and climate: an update in the light of the current exceptional solar minimum, P. Roy. Soc. A-Math Phy., 466, 303–329, 2010.
43. Lockwood, M.: Reconstruction and prediction of variations in the open solar magnetic flux and interplanetary conditions, Living Rev. Sol. Phys., 10, 4, 2013.
44. Maleski, J. J. and Martinez, C. J. (2018), Coupled impacts of ENSO AMO and PDO on temperature and precipitation in the Alabama–Coosa–Tallapoosa and Apalachicola–Chattahoochee–Flint river basins. Int. J. Climatol, 38: e717-e728. doi:10.1002/joc.5401
45. Mantua, N. J., Hare, S. R., Zhang, Y., Wallace, J. M., and Francis, R. C.: A Pacific interdecadal climate oscillation with impacts on salmon production, B. Am. Meteorol. Soc., 78, 1069–1079, 1997.
46. Mantua, N. J., and Hare, S. R.: The Pacific Decadal Oscillation, J. Oceanogr., 58, 35–44, 2002.
47. McKinley, G. A., Takahashi, T., Buitenhuis, E., Chai, F., Christian, J. R., Doney, S. C., Jiang, M.-S., Lindsay, K., Moore, J.K, Le Quéré, C., Lima, I., Murtugudde, R., Shi, L., and Wetzel, P.: North Pacific carbon cycle response to climate variability on seasonal to decadal timescales, J. Geophys. Res., 111, C07S06, doi:10.1029/2005JC003173, 2006.
48. Montecino, V., and Lange, C. B.: The Humboldt Current System: Ecosystem components and processes, fisheries, and sediment studies, Prog. Oceanogr., 83, 65-79, 2009.

49. Monteith, J. L.: Solar Radiation and Productivity in Tropical Ecosystems, J. App. Ecol., 9, 747-66, doi:10.2307/2401901, 1972.

50. Montgomery, D. C., Peck, E. A. and Vining, G. G. (2001). Introduction to Linear Regression Analysis. 3rd Edition, New York, New York: John Wiley & Sons.

51. Mörner, N.-A.: The Approaching New Grand Solar Minimum and Little Ice Age Climate Conditions, Natural Science, 7, 510-518, doi: 10.4236/ns.2015.711052, 2015.

52. Newman, M., Compo, G. P., and Alexander, M. A.: ENSO-forced variability of the Pacific decadal oscillation, J. Climate, 16, 3853-3857, doi: 10.1175/1520-0442(2003)016<3853: EVOTPD>2.0.CO;2., 2003.

53. Ormaza-González, F.I., and Cedeño, J.: Coastal El Niño 2017 or Simply: The Carnival Coastal Warming Event? MOJ Ecology & Environmental Sciences, 2, 00054, doi: 10.15406/mojes.2017.02.00054, 2017.

54. Ormaza-González, F. I., and Sánchez, E.: Cálculo computacional del flujo de energía solar cobre el océano y su aplicación a la zona ecuatorial, Rev. Ciencias del Mar y Limnología (INP-Ecuador), 2(1), 27-54, ISSN 1390-5767, 1983.

55. Ormaza-González, F. I., Mora, A., Bermúdez, R. M., Hurtado, M. A., Peralta, M. R., and Jurado, V. M.: Can small pelagic fish landings be used as predictors to high frequency oceanographic fluctuations in the 1-2 El Niño region? Adv. Geosci., 42, 61–72, doi:10.5194/adgeo-42-61-2016, 2016a.

56. Ormaza-González, F. I., Mora, A., and Bermúdez, R. M.: Relationships between tuna catch and variable frequency oceanographic conditions, Adv. Geosci., 42, 83–90, doi:10.5194/adgeo-42-83-2016, 2016b.

57. Rasmussen, E. M., and Carpenter, T. H.: Variations in tropical sea surface temperature and surface wind fields associated with the Southern Oscillation/El Niño, Mon. Weather Rev., 110, 354-384, 1982.

58. Scafetta, N.: Global temperatures and sun spot numbers. Are they related? Yes, but non-linearly. A reply to Gil-Alana et al. (2014), Physica A., 413, 329-342, doi: 10.1016/j.physa.2014.06.047, 2014.
59. Shindell, D. T., Schmidt, G. A., Mann, M. E., Rind, D., and Waple, A.: Solar Forcing of Regional Climate Change During the Maunder Minimum, Science, 294 (5549), 2149-2152, doi: 10.1126/science.1064363, 2001.
60. Schlesinger, M. E., and Ramankutty, N.: An oscillation in the global climate system of period 65–70 years, Nature, 367, 723–726, doi:10.1038/367723a0., 1994.
61. Smyth, T. J. 2011. Penetration of UV irradiance into the global ocean. J. Geophys. Res., 116C11020, doi:10.1029/2011JC007183.
62. Trenberth, K.E., Fasullo, J.T., and Balmaseda, M.A.: Earth's Energy Imbalance, J. Climate, 27, 3129–3144, doi:10.1175/JCLI-D-13-00294.1, 2014.
63. van Oldenborgh, G. J., te Raa, L. A., Dijkstra, H. A., and Philip, S. Y.: Frequency- or amplitude-dependent effects of the Atlantic meridional overturning on the tropical Pacific Ocean, Ocean Sci., 5, 293-301, doi:10.5194/os-5-293-2009, 2009.
64. van Loon, H., Meehl, G. A., and Shea, D. J.: Coupled air-sea response to solar forcing in the Pacific region during northern winter, J. Geophys. Res., 112D02108, doi:10.1029/2006JD007378, 2007.
65. Wang, G., Cheng, L., Abraham, J., and Li, C.: Consensuses and discrepancies of basin-scale ocean heat content changes in different ocean analyses, Clim. Dynam., doi:10.1007/s00382-017-3751-5, 2017.
66. Wenjuan, H., and XIAO, Z.: The impact of solar activity on the 2015/16 El Niño event, Atmospheric and Oceanic Science Letters, doi:10.1080/16742834.2016.1231567, 2016.
67. White, W. B., Lean, J., Cayan, D. R., and Dettinger, M. D.: Response of global upper ocean temperature to changing solar irradiance, J. Geophys. Res., 102(C2), 3255–3266, doi:10.1029/96JC03549, 1997.

68. Wolter, K., and Timlin, M.S.: Monitoring ENSO in COADS with a seasonally adjusted principal component index, Proceedings of the 17th Climate Diagnostics Workshop, 52-57, Norman, OK, 1993.

69. Wolter, K., and Timlin, M. S.: Measuring the strength of ENSO events - how does 1997/98 rank? Weather, 53, 315-324, 1998.

70. Wolter, K., and Timlin, M. S.: El Niño/Southern Oscillation behaviour since 1871 as diagnosed in an extended multivariate ENSO index (MEI.ext), Int. J. Climatol., 31, 1074–1087, doi:10.1002/joc.2336, 2011.

71. Yamakawa, S., Makoto, I., and Ramasamy, S.: Relationships between solar activity and variations in SST and atmospheric circulation in the stratosphere and troposphere, Quatern. Int., 397, 289-299, 2016.

72. Yim, B. Y., Noh, Y., Yeh, S. -W., Kug, J. -S., Min, H. S., and Qiu, B.: Ocean mixed layer processes in the Pacific Decadal Oscillation in coupled general circulation models, Clim. Dynam, 41, 1407–1417, doi: 10.1007/s00382-012-1630-7, 2013.

73. Yoon, J., and Yeh, S. -W.: Influence of the Pacific Decadal Oscillation on the Relationship between El Niño and the Northeast Asian Summer Monsoon, J. Climate, 23, 4525–4537, doi:10.1175/2010JCLI3352.1, 2010.

74. Yuan, Y., and Yan, H.: Different types of La Niña events and different responses of the tropical atmosphere, Chinese Sci. Bull., 58, 406–415, doi:10.1007/s11434-012-5423-5, 2012.

75. Zhang, Y., Wallace, J. M., and Battisti, D. S.: ENSO-like Interdecadal Variability: 1900–93, J. Climate, 10, 1004-1020, 1997.

76. Zheng, F., Fang, X.-H., Zhu, J., Yu, J.-Y., and Li, X.-C.: Modulation of Bjerknes feedback on the decadal variations in ENSO predictability, J. Geophys. Res. Lett., 43, 560–568, doi:10.1002/2016GL07163, 2016.

77. Zhou, J., and Tung, K. -K.: Solar Cycles in 150 Years of Global Sea Surface Temperature Data, J. Climate, 23, 3234-3248, 2010.

78. Zong, Z., Yong, L., and Jian, H.: Effects of Sunspot on the Multi-Decadal Climate Projections, Advances in Climate Change Research, 5, 51-56, doi:10.3724/SP.J.1248.2014.051, 2014.

Table 1. Linear correlations (r^2 and p-values) between SS monthly counts and PDO, MEI, ONI, AMO, SST and SST Anomaly in 1+2, and 3.4 for the period April 1954 to December 2017. Negative r^2 means negative slopes of the linear regression curves.

Variable		**(t+0)**	**(t+6)**	**(t+12)**	**(t+24)**	**(t+36)**	**(t+48)**
PDO	r^2	0.00	0.02	0.04	0.04	0.03	0.02
	p-value	3.83E-01	1.75E-04	1.94E-07	1.26E-08	2.07E-06	3.11E-05
MEI	r^2	0.01	0.02	0.03	0.02	0.01	0.00
	p-value	2.58E-02	9.68E-05	2.55E-06	1.63E-05	1.51E-02	9.30E-01
ONI	r^2	0.01	0.03	0.04	0.03	0.01	0.00
	p-value	2.22E-03	4.93E-06	2.11E-07	1.91E-06	4.00E-03	4.13E-01
AMO	r^2	0.00	-8.30E-04	-9.66E-04	-2.89E-03	0.01	0.02
	p-value	7.97E-01	4.28E-01	3.94E-01	1.44E-01	1.45E-03	2.21E-04
SST 1+2	r^2	-2.54E-04	1.61E-03	-3.08E-05	-2.92E-06	-3.04E-04	-1.26E-03
	p-value	6.61E-01	2.71E-01	8.80E-01	9.63E-01	6.37E-01	3.44E-01
SSTA 1+2	r^2	0.00	0.00	0.00	0.00	0.00	-0.00
	p-value	7.14E-01	1.67E-01	3.37E-01	2.57E-01	8.13E-01	3.73E-01
SST 3.4	r^2	0.00	0.01	0.01	0.01	0.00	-0.00
	p-value	2.78E-01	5.93E-03	1.07E-03	1.32E-03	6.48E-02	9.10E-01
SSTA 3.4	r^2	0.00	0.01	0.02	0.02	0.01	0.00
	p-value	1.45E-01	2.25E-03	8.23E-05	1.23E-04	2.45E-02	9.79E-01

Fig. 1. Behaviour of monthly counts of SS, ONI, MEI, PDO and AMO. The indexes start at t= 0, 12, 24 and 36 months (panels a, b, c and d respectively). The SS series starts at t=0 in the four panels. The vertical axis gives the values for the indexes and SS numbers (multiply by 100).

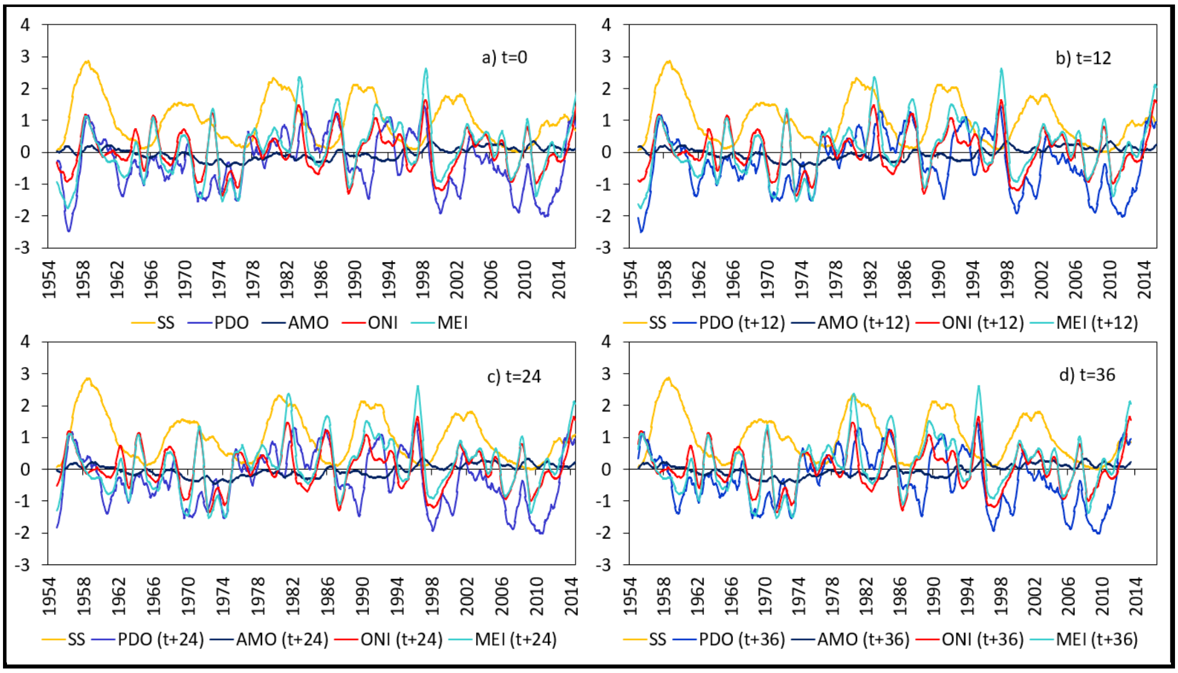

Fig. 2. Linear regression correlation coefficient r^2 ($p<0.05$) of SS monthly counts against SST Anomaly in regions El Niño 1+2 (blue) and 3.4 (red) and indexes PDO (grey) and ONI (green) through three time periods.

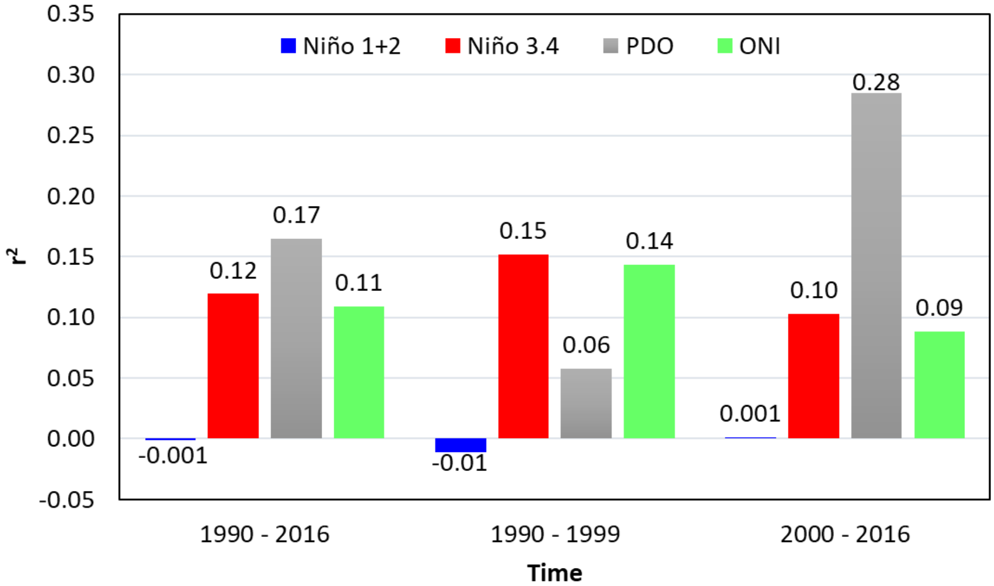

Fig. 3. Linear regression correlation coefficient r^2 ($p<0.05$) of SS monthly counts for cycles 19-24 against SST in regions El Niño 1+2 (blue) and 3.4 (red).

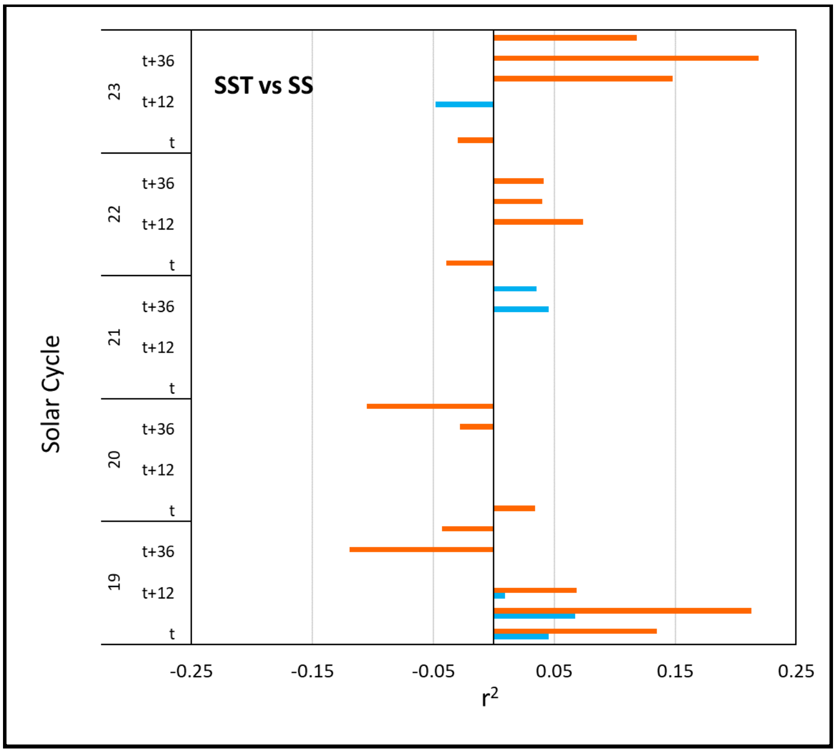

Fig. 4. Linear regression correlation coefficient r^2 ($p<0.05$) of SS monthly counts of cycles 19-24 against SST Anomaly in regions El Niño 1+2 (blue) and 3.4 (red).

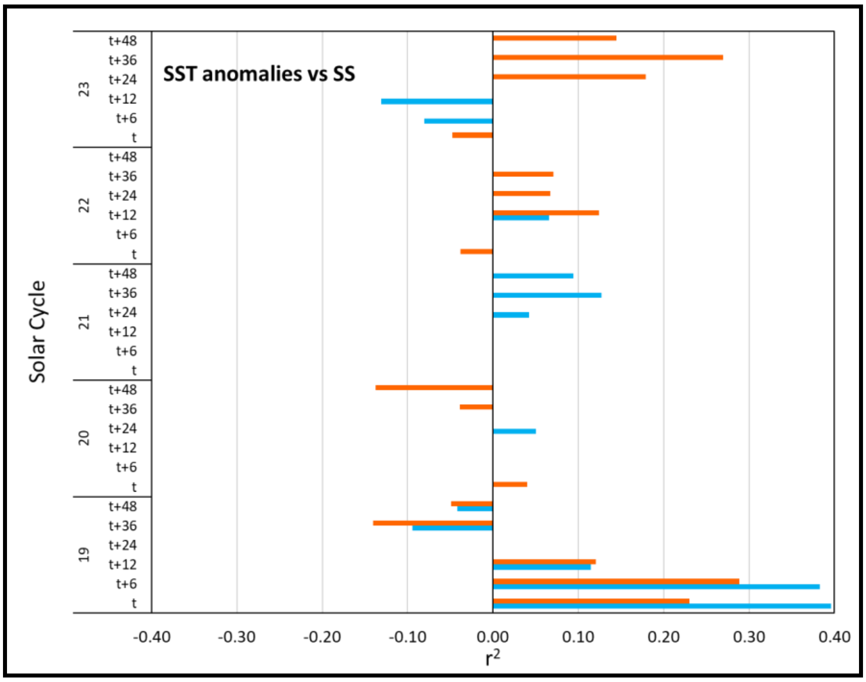

Fig. 5. Linear regression correlation coefficient r^2 ($p<0.05$) of SS monthly counts cycles 19-24 against indexes: ONI (red) and PDO (blue). Negative slope ($- r^2$).

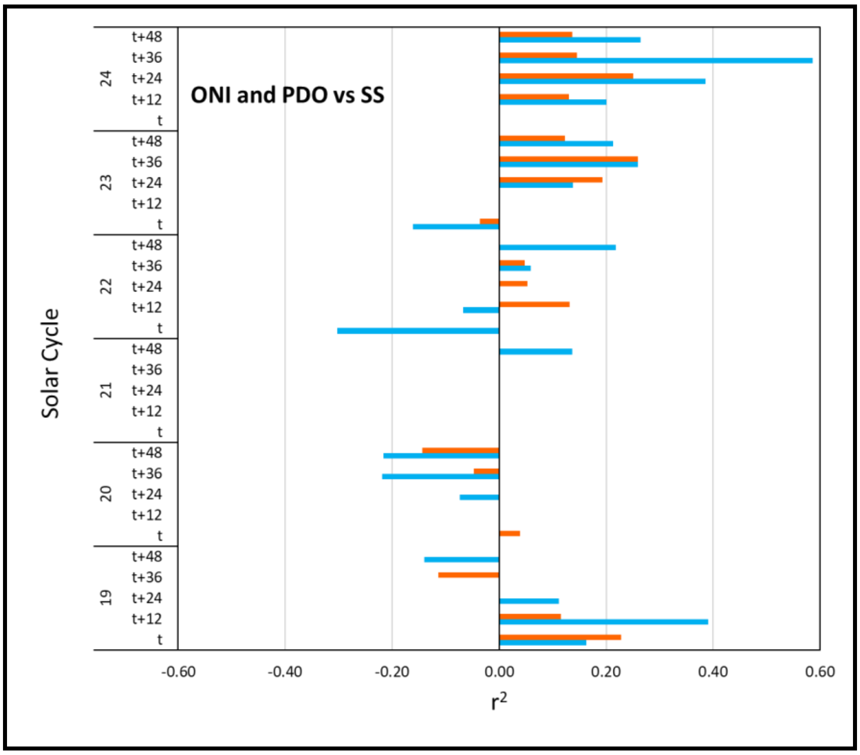

Fig. 6. Linear regression correlation coefficient r^2 ($p<0.05$) of SS monthly counts for cycles 19-24 against index AMO. Negative slope ($-r^2$).

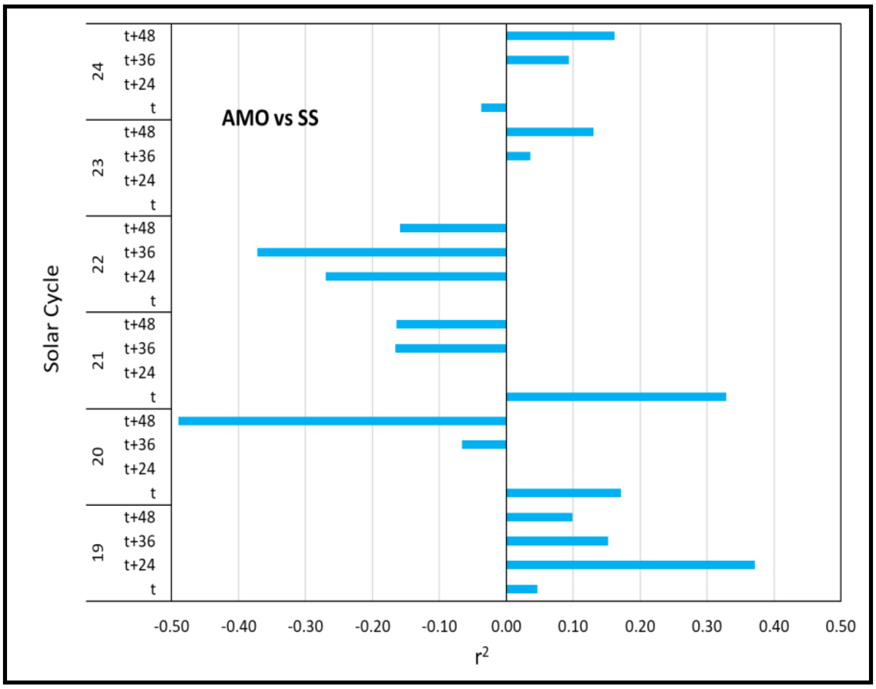

Fig. 7. Linear regression correlation coefficient r^2 ($p<0.05$) of SS monthly counts during the ascending (blue) and descending (red) phases of SS for cycles 19-24 against SST in regions El Niño 1+2 (left) and 3.4 (right).

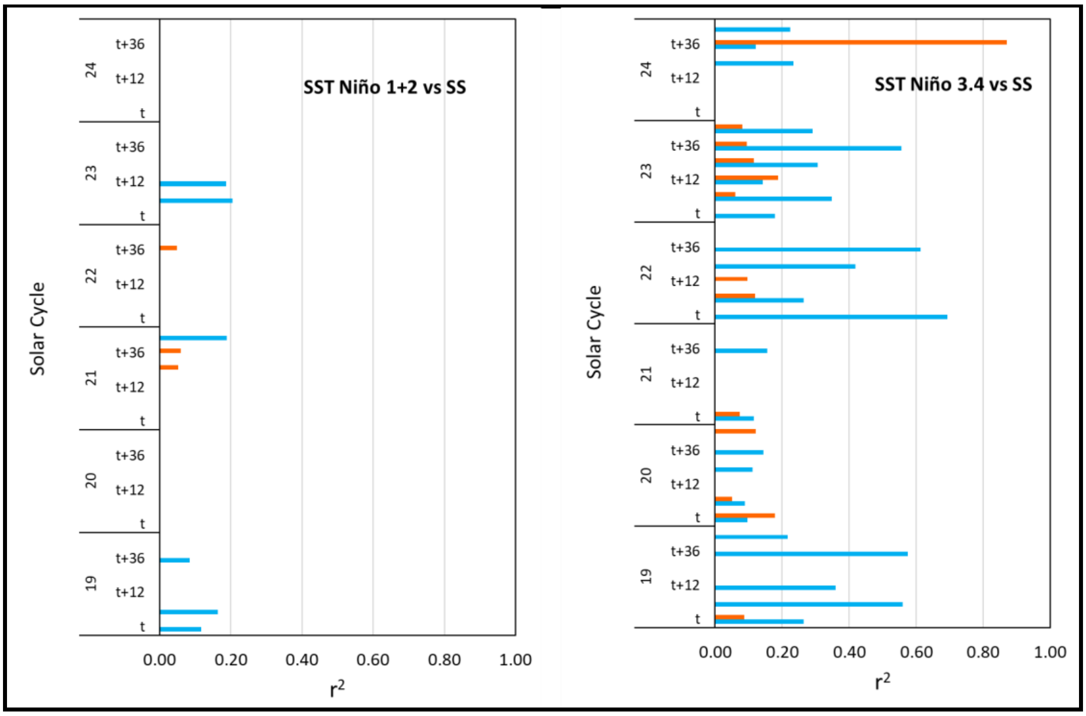

Fig. 8. Linear regression correlation coefficient r^2 ($p<0.05$) of SS monthly counts during the ascending (blue) and declining (red) phases for SS cycles 19-24 against SST Anomaly in regions El Niño 1+2 (left) and 3.4 (right).

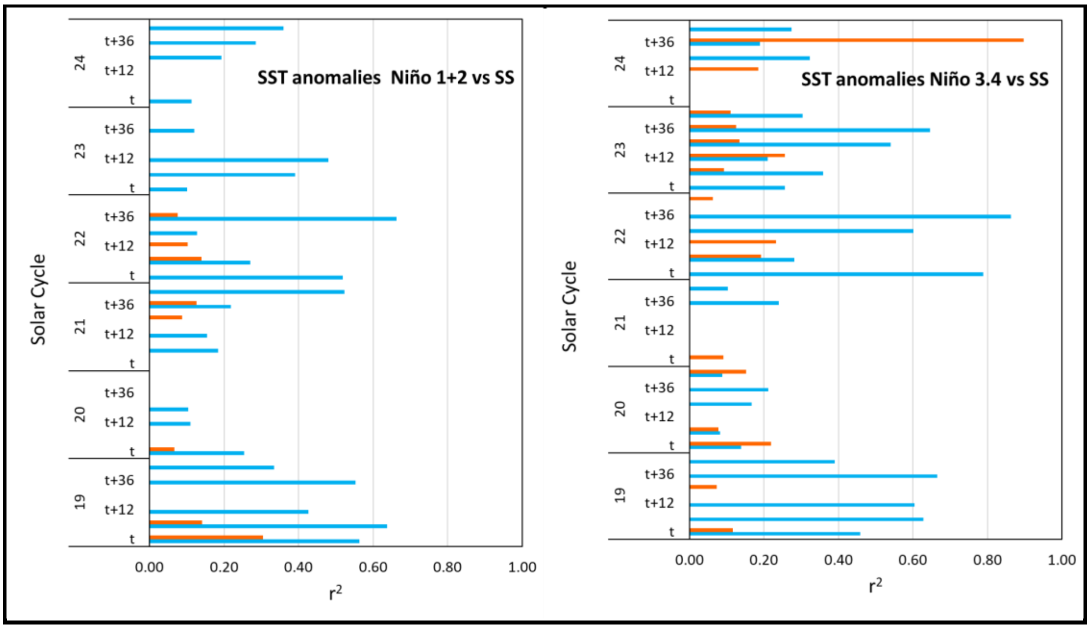

Fig. 9. Linear regression correlation coefficient r^2 of SS monthly counts during the ascending (blue) and declining (red) phases of SS cycles (19-24) against index ONI. Negative slope (- r^2).

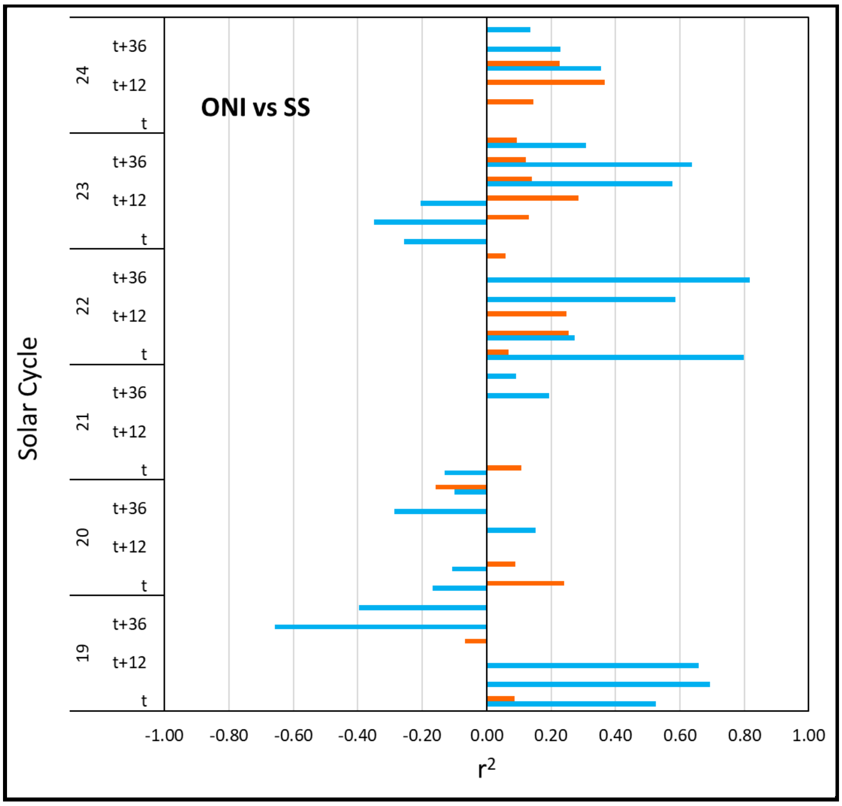

Fig. 10. Linear regression correlation coefficient r^2 ($p<<0.05$) of SS monthly counts during the ascending (blue) and declining (red) phases of SS cycles (19-24) against index PDO. Negative slope (- r^2).

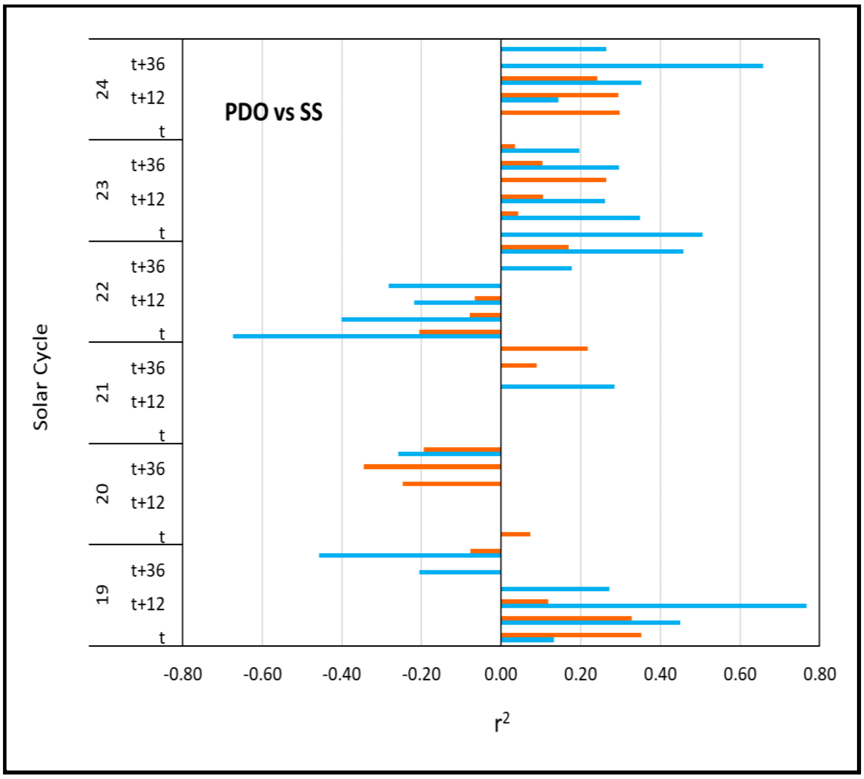

Fig. 11. Linear regression correlation coefficient r^2 of SS numbers during the ascending (blue) and declining (red) phases of SS cycles (19-24) against index AMO. Negative slope ($-r^2$)

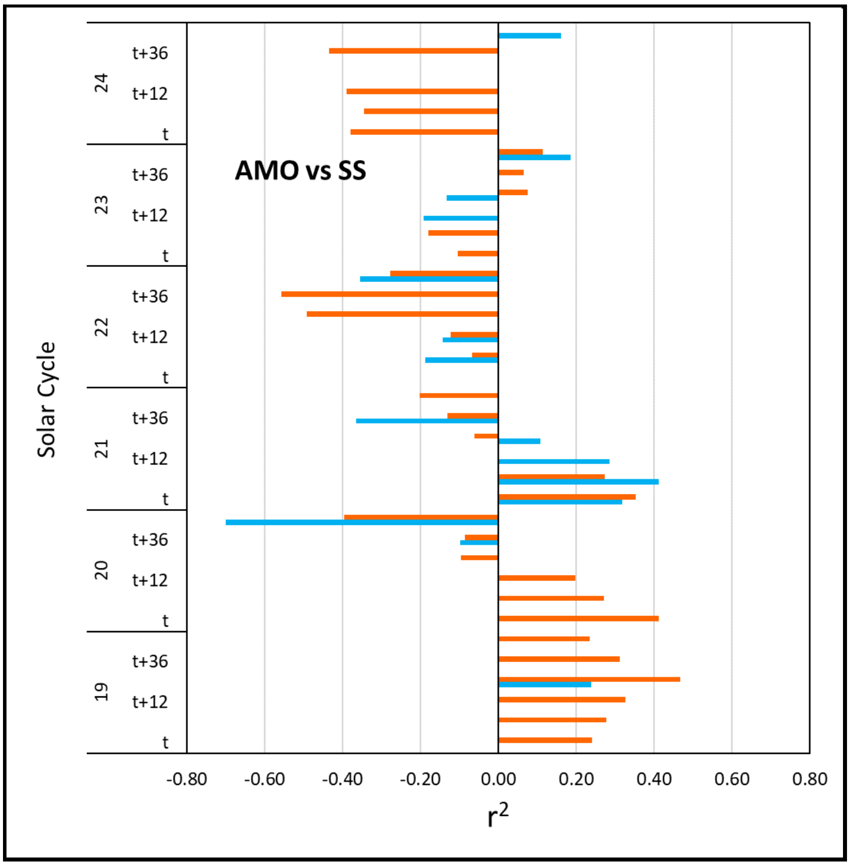

Fig. 12. Polynomial functions of 6 degrees (p<0.001), based on monthly SS counts. Red and blue lines represent El Niño and La Niña event. The cycle number of the top of each panel.